ACS Synthetic Biology

pubs.acs.org/synthbio
Research Article

Directed Evolution of Acoustic Reporter Genes Using High-Throughput Acoustic Screening

Robert C. Hurt,[⊥] Zhiyang Jin,[⊥] Mohamed Soufi, Katie K. Wong, Daniel P. Sawyer, Hao K. Shen, Przemysław Dutka, Ramya Deshpande, Ruby Zhang, David R. Mittelstein, and Mikhail G. Shapiro*

Cite This: ACS Synth. Biol. 2024, 13, 2215−2226

ABSTRACT: A major challenge in the fields of biological imaging and synthetic biology is noninvasively visualizing the functions of natural and engineered cells inside opaque samples such as living animals. One promising technology that addresses this limitation is ultrasound (US), with its penetration depth of several cm and spatial resolution on the order of 100 μm. Within the past decade, reporter genes for US have been introduced and engineered to link cellular functions to US signals *via* heterologous expression in commensal bacteria and mammalian cells. These acoustic reporter genes (ARGs) represent a novel class of genetically encoded US contrast agent, and are based on air-filled protein nanostructures called gas vesicles (GVs). Just as the discovery of fluorescent proteins was followed by the improvement and diversification of their optical properties through directed evolution, here we describe the evolution of GVs as acoustic reporters. To accomplish this task, we establish high-throughput, semiautomated acoustic screening of ARGs in bacterial cultures and use it to screen mutant libraries for variants with increased nonlinear US scattering. Starting with scanning site saturation libraries for two homologues of the primary GV structural protein, GvpA/B, two rounds of evolution resulted in GV variants with 5- and 14-fold stronger acoustic signals than the parent proteins. We anticipate that this and similar approaches will help high-throughput protein engineering play as large a role in the development of acoustic biomolecules as it has for their fluorescent counterparts.

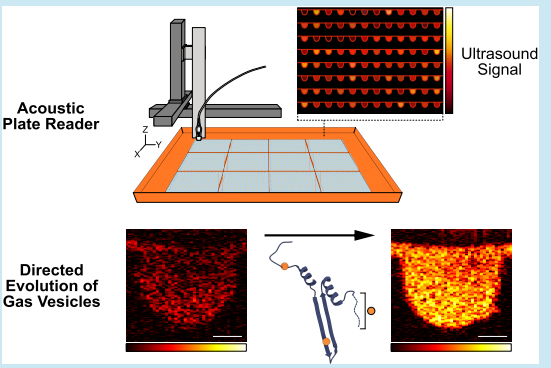

KEYWORDS: *gas vesicles, acoustic reporter genes, ultrasound, directed evolution, high-throughput screening*

INTRODUCTION

Acoustic reporter genes (ARGs)—genetically encoded reporters that enable the imaging of gene expression using ultrasound (US)—were first introduced to bacteria in 2018[1] and subsequently to mammalian cells in 2019.[2] ARGs are based on genetically encoded, gas-filled protein nanostructures called gas vesicles (GVs), which evolved as intracellular flotation devices allowing aerophilic and photosynthetic bacteria to float to oxygenated and better-lit surface waters.[3,4] GVs scatter US due to the difference in the density and compressibility of their gaseous interior relative to a surrounding aqueous medium.[5] GVs have been the subject of intense study,[4−11] development,[12] and application[13−22] in recent years.[23−25] ARGs have received considerable attention due to their ability to enable noninvasive, long-term, real-time imaging of gene expression in both bacterial and mammalian cells deep inside living organisms: in particular, ARGs have been used to image tumor growth[2,12] and colonization by therapeutic bacteria,[12] protease activity,[13] phagolysosomal function,[6] and intracellular Ca^{2+} dynamics.[7] However, despite several successful efforts to engineer the acoustic and expression properties of ARGs, further improvements to the performance of ARGs are needed to enable their most impactful applications—in particular, those requiring the highly sensitive and specific detection of ARGs expressed by bacterial or mammalian cells, such as in gut microbiome or tumor imaging.

Unfortunately, the methods currently available for ARG engineering and acoustic characterization are low-throughput, complex to implement, and require a great deal of hands-on time per sample. In particular, manual loading and imaging of individual samples limits throughput to a handful of samples per day. In contrast, the state-of-the-art high-throughput methods used to engineer fluorescent proteins can process far larger libraries in shorter times, with less intervention from users: plate readers can assay thousands of samples per run, and flow cytometers have been used to screen libraries of 10^8

Received: April 22, 2024
Revised: June 24, 2024
Accepted: June 27, 2024
Published: July 9, 2024

https://doi.org/10.1021/acssynbio.4c00283
ACS Synth. Biol. 2024, 13, 2215−2226

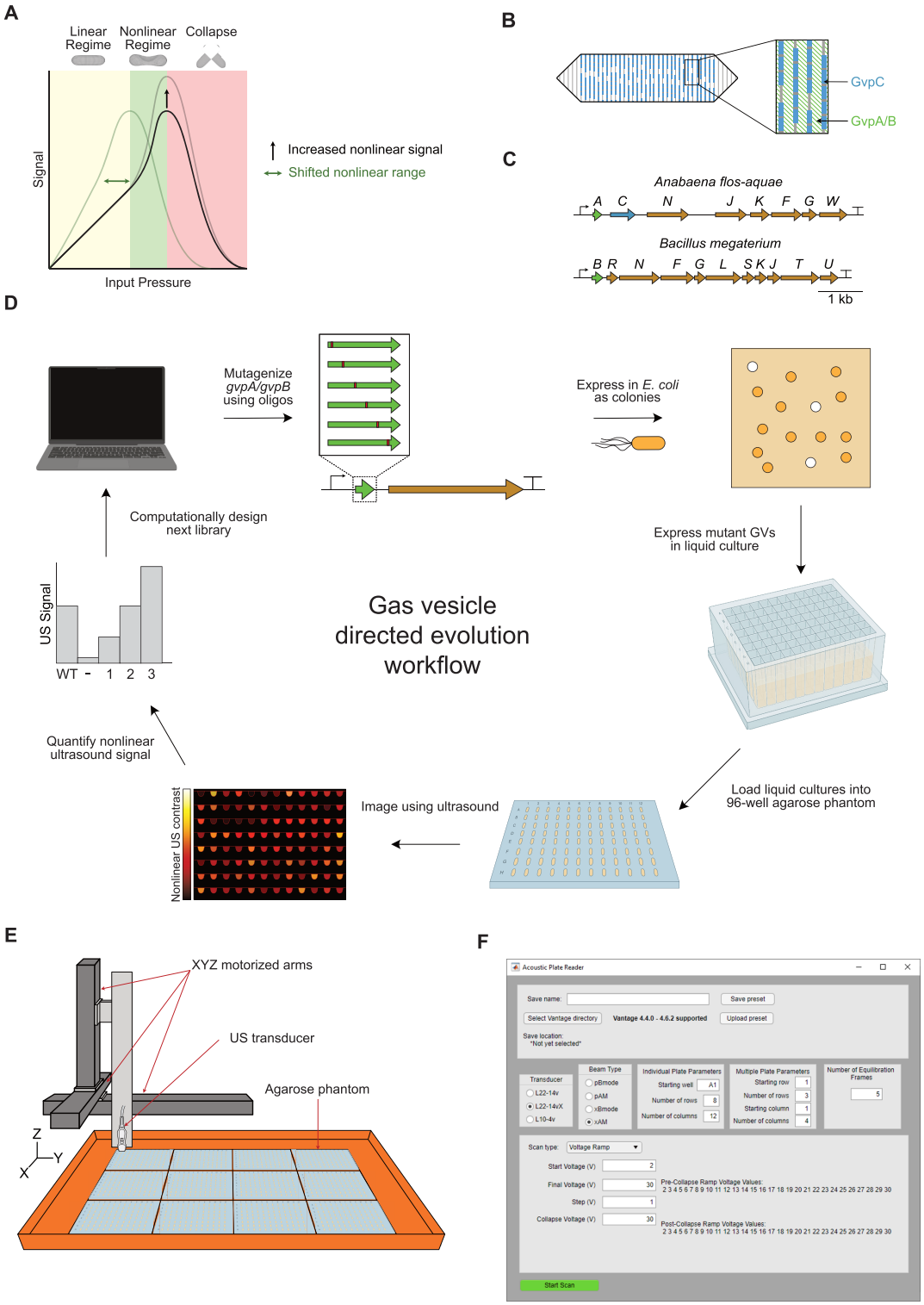

Figure 1. High-throughput directed evolution workflow for ARGs. (A) Three regimes of GV response to US. (B) Roles of the structural proteins GvpA/B and GvpC in GV structure. (C) Diagrams of the gene clusters used as starting points for evolution. (D) Schematic of directed evolution workflow for ARGs. The starting point GV structural protein is mutagenized, then expressed in *Escherichia coli* as colonies on Petri dishes. Colonies that turn white are assumed to produce GVs, and are picked and expressed in liquid culture. Cultures of GV-expressing *E. coli* are then loaded into agarose phantoms and imaged using US at 15.625 MHz. The resulting nonlinear US intensity data are used to rank the performance of mutants and select the most promising ones for further mutagenesis. (E) Schematic of the Acoustic Plate Reader (APR), which is used for automated US image collection of up to 1152 samples of GV-expressing *E. coli* arrayed in 96-well agarose phantoms. (F) Image of the graphical user interface for the APR.

mutants in a single experiment.[8] In the past few decades, a growing suite of protein engineering techniques have been developed[9] and applied with remarkable success to improving fluorescent proteins, opsins, Cas proteins, and other bio-

https://doi.org/10.1021/acssynbio.4c00283
ACS Synth. Biol. 2024, 13, 2215−2226

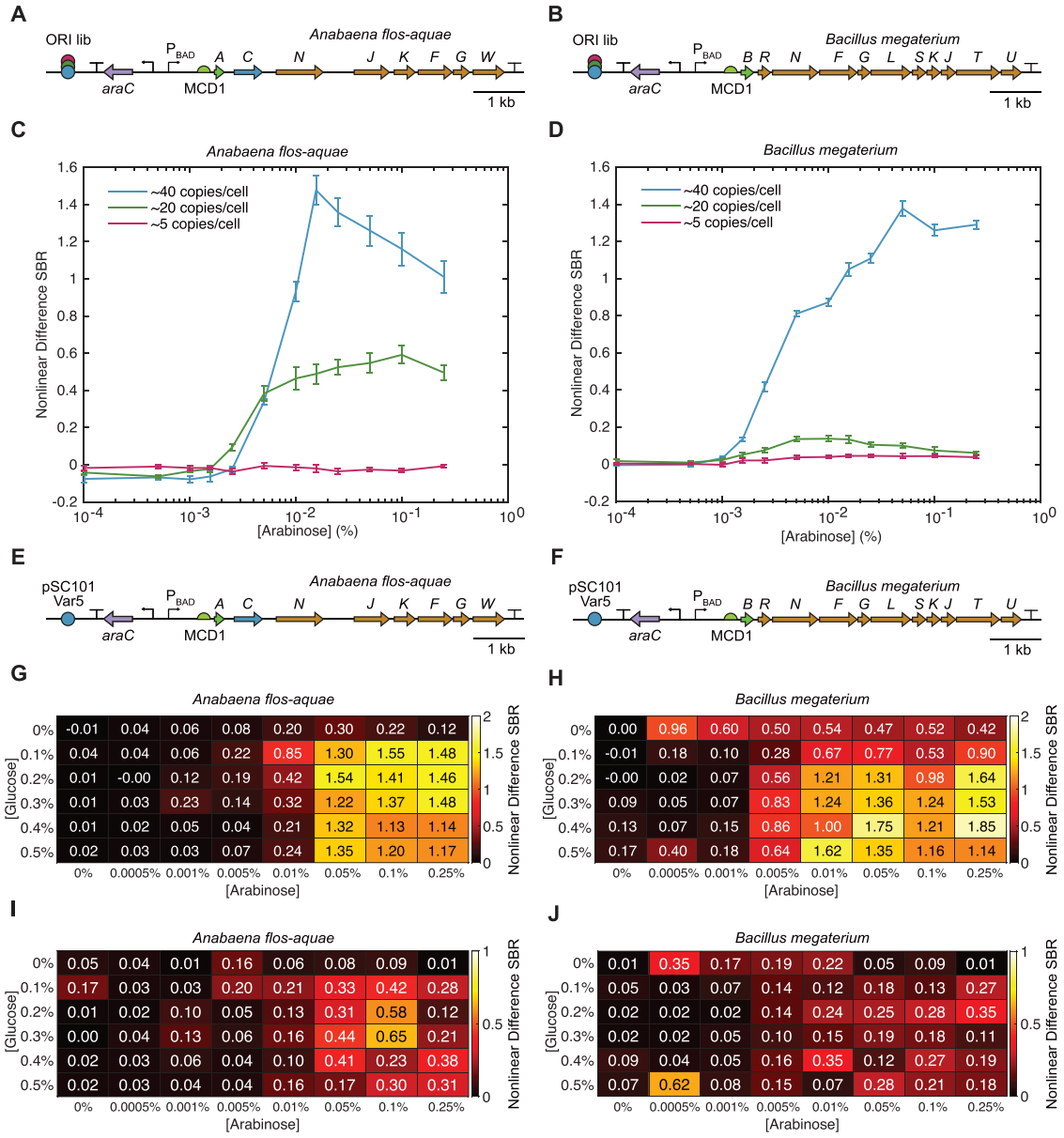

Figure 2. Optimization of GV expression from the WT *A. flos-aquae* and *B. megaterium* gene clusters. (A, B) Diagrams of the WT *A. flos-aquae* and *B. megaterium* gene clusters with libraries of origins of replication (ORIs) of different strengths. (C, D) Nonlinear US signal produced from expression of both clusters at three different copy numbers as a function of inducer concentration. The nonlinear difference SBR is the difference in signal-to-background ratio between pre- and postcollapse images of each sample (see Methods Section for details). Error bars represent standard error. $N = 8$ biological samples (each an average of 3 technical replicates). (E, F) Diagrams of the optimized WT *A. flos-aquae* and *B. megaterium* gene clusters used for directed evolution, both of which used the pSC101-Var5 ORI (~40 copies/cell). (G, H) Mean and (I, J) STD of the nonlinear US signal produced by both WT clusters as a function of the concentrations of glucose and arabinose used for autoinduction. The concentrations selected for GV expression during library screening were 0.25% glucose and 0.05% arabinose. $N = 3$ biological samples (each an average of 3 technical replicates).

technology tools, but these methods often require the screening of libraries containing thousands of members or more.[10] Thus, the low throughput of current acoustic screening methods prevents the effective use of most of the tools needed to unlock the full potential of ARGs.

In this study, we developed a high-throughput, semi-automated pipeline for acoustic screening of ARGs, and used it to evolve two ARG clusters to improve their nonlinear acoustic signals. Our acoustic plate reader (APR) system is capable of collecting acoustic data on up to 1152 ARG samples in a single automated scan, and includes graphical user interfaces (GUIs) for data collection and processing. The APR workflow facilitates faster, more reliable, and more standardized acoustic screening of ARG samples, requiring significantly less hands-on time than current methods. Using this pipeline, we improved the nonlinear acoustic signal produced by two ARG clusters—derived from *Anabaena flos-aquae* and *Bacillus megaterium*—by 5- and 14-fold, respectively, when expressed at physiological temperature. Microscopy revealed that these evolved ARG clusters produce more GVs per cell than their parents.

https://doi.org/10.1021/acssynbio.4c00283
ACS Synth. Biol. 2024, 13, 2215−2226

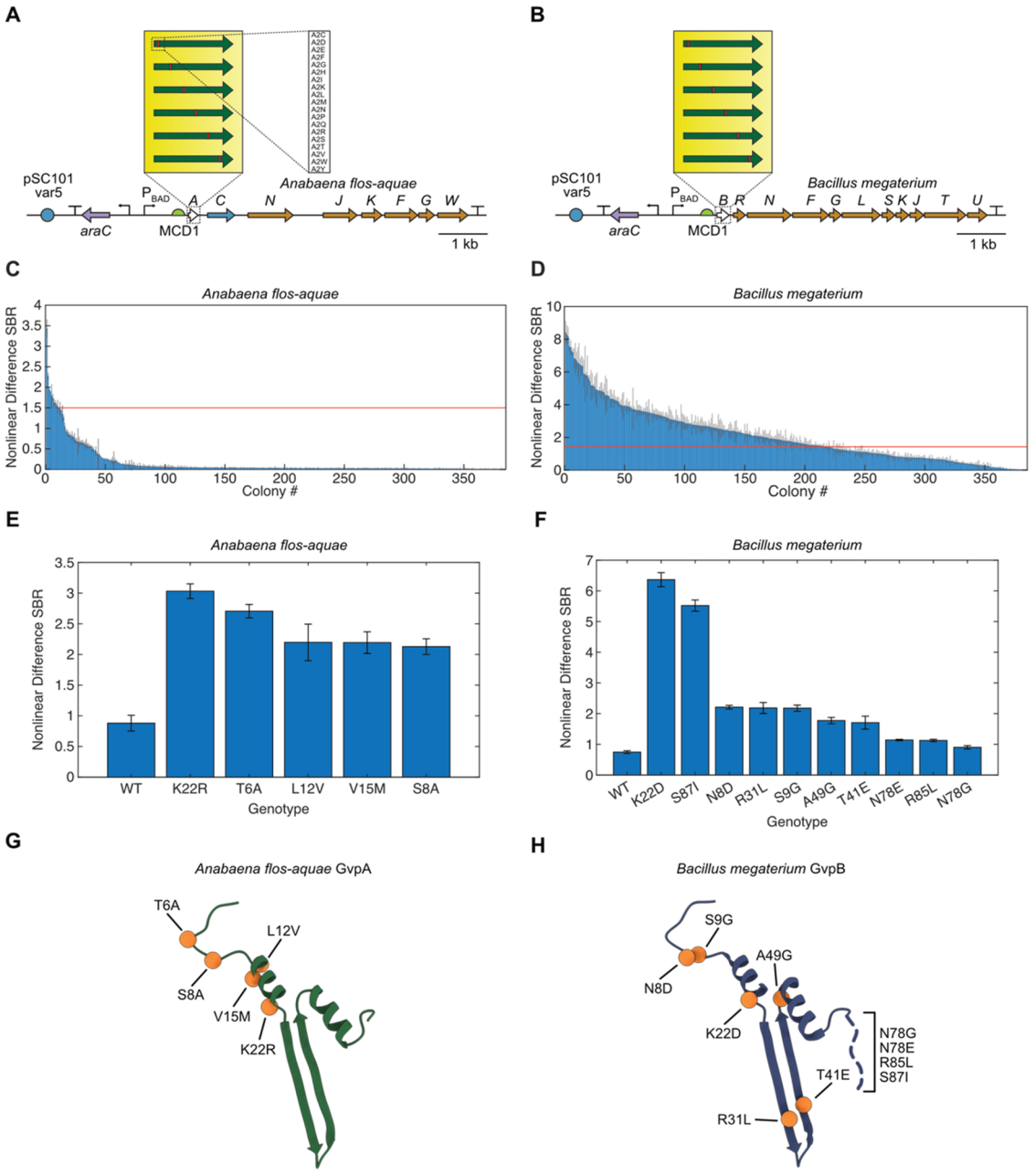

Figure 3. First round of directed evolution of *A. flos-aquae* and *B. megaterium* structural proteins. (A, B) Diagrams of the mutagenized *A. flos-aquae* and *B. megaterium* gene clusters, depicting the scanning site saturation libraries screened in the first round of evolution. (C, D) Nonlinear US difference signal-to-background ratio (SBR) from all screened mutants of both clusters. Red lines indicate the nonlinear difference SBR of the WT for that cluster. Error bars represent standard error. $N = 3$ technical replicates of one biological sample. (E, F) Nonlinear US difference SBR for the WT and top mutants for each cluster. Error bars represent standard error. $N = 4$ biological samples (each an average of 3 technical replicates). (G, H) Locations of top mutations from (E, F) in the GvpA/GvpB structure (PDB 8GBS and 7R1C).

RESULTS AND DISCUSSION

A High-Throughput Directed Evolution Workflow for ARGs. GVs are known to respond to US in three regimes, depending on the input pressure applied: linear scattering, nonlinear scattering, and collapse[11,22] (Figure 1A). Of particular interest for *in vivo* imaging is the nonlinear scattering regime in which GVs produce significantly more contrast than tissue, putatively by "buckling" of their shells.[11,19−22] This effect has been exploited previously to nondestructively image GV-expressing bacterial and mammalian cells *in vivo* with high specificity,[12] and enhancing this nonlinear US scattering phenotype is a top priority of current ARG engineering efforts.

The primary GV structural protein—GvpA or its homologue GvpB—creates the cone-tipped cylindrical body of the GV, and optionally GvpC may attach to the outside of this structure and reinforce it mechanically (Figure 1B). It has already been shown that engineering GvpC to reduce its binding to GvpA can result in GVs with increased nonlinear signal or decreased collapse pressure,[18] but GvpC serves as a limited target for engineering these phenotypes because not all GV types include GvpC. We chose to explore whether altering the primary structure of the main GV structural protein—GvpA in the *A. flos-aquae* cluster and GvpB in the *B. megaterium* cluster—could increase the amount of nonlinear US contrast produced

https://doi.org/10.1021/acssynbio.4c00283
ACS Synth. Biol. 2024, 13, 2215−2226

by *E. coli* expressing either ARG type. We selected the GV gene clusters obtained from these species as our starting points based on the previous use of the *B. megaterium* cluster as a bacterial ARG[1] and the use the *A. flos-aquae* cluster in reconstituted contrast agents and mammalian ARGs,[2,7,18] making it desirable to obtain its efficient bacterial expression. Starting without the benefit of the recently published structures and structural models of these proteins,[16,17] we chose an approach based on random mutagenesis and high-throughput acoustic screening of ARG mutants.

As starting points for evolution, we chose the minimal versions of the WT *B. megaterium* ATCC 19213 cluster[15] (lacking *gvpA*, *gvpP*, and *gvpQ*) and the WT *A. flos-aquae* cluster (with only one copy of *gvpA*, and lacking *gvpV*) (Figure 1C). To engineer the desired nonlinear signal and collapse pressure phenotypes, we developed a method for high-throughput, semiautomated characterization of US contrast and GV collapse pressure in *E. coli* (Figure 1D).

First, we constructed scanning site saturation libraries of *gvpA* or *gvpB* in these clusters, and performed a selection for high levels of GV expression by inducing transformants on Petri dishes and picking only colonies that appeared white (GV-expressing bacteria appear white because GVs scatter light, in addition to US).[14,24] These mutants were then expressed in liquid cultures in 96-well format and loaded into agarose phantoms. We imaged these phantoms using an automated scanning setup in which a software-controlled three-dimensional (3D) translating stage raster-scans an US transducer above the submerged phantoms (Figure 1E), producing a set of US images in which samples with high GV expression appear bright. This pipeline allowed us to generate and acoustically screen several mutant libraries, from which we identified mutants with significantly enhanced acoustic phenotypes. We also created graphical user interfaces (GUIs) to simplify and standardize data acquisition (Figure 1F) and analysis. We termed this setup the "Acoustic Plate Reader" (Figure S1 and Video S1).

Optimizing GV Expression from WT *A. flos-aquae* and *B. megaterium* Gene Clusters. Before engineering the structural proteins, we optimized the expression of the WT *A. flos-aquae* and *B. megaterium* gene clusters in *E. coli* at 37 °C. For each cluster, we cloned three origins of replication (ORIs) of different strengths (~40, ~20, and ~5 copies/cell)[25] (Figure 2A,B), and assessed their performance in liquid culture as a function of inducer concentration. For both clusters, the strongest ORI tested gave the highest nonlinear US signal (Figure 2C,D), and was chosen for future experiments. With the optimal ORIs selected for expression (Figure 2E,F), we then sought to optimize the autoinduction conditions to maximize nonlinear signal (in autoinduction media, increasing the concentration of glucose increases the cell density at which induction occurs, while increasing the concentration of the inducing sugar increases the level to which the transcription unit is induced). We performed titrations of glucose and arabinose and assessed the resulting nonlinear signal from the expressed constructs (Figure 2G,H); we decided on concentrations of 0.25% glucose and 0.05% arabinose for induction of these constructs in future experiments, as these conditions yielded high GV expression from both constructs while leaving enough induction dynamic range to tune the expression levels of mutants later without the need to alter any regulatory elements. We observed that the US signal from the *A. flos-aquae* cluster peaked at a moderate arabinose concentration (Figure 2C,G), while expression from the *B. megaterium* cluster was highest at the maximum concentration (Figure 2D,H). We suspect that the signal decline from the *A. flos-aquae* cluster at high arabinose concentrations is due to the high metabolic burden associated with expressing so many non-native proteins in *E. coli*.

Round 1 Directed Evolution of *A. flos-aquae* GvpA and *B. megaterium* GvpB. To improve the nonlinear signal from the WT *A. flos-aquae* and *B. megaterium* clusters in *E. coli*, we designed scanning site-saturation libraries of the genes encoding the primary GV structural protein for each (*i.e.*, *gvpA* for *A. flos-aquae*; *gvpB* for *B. megaterium*) (Figures 3A,B and S2A). This resulted in libraries containing 1400 and 1740 members for *gvpA* and *gvpB*, respectively (Table S1, Library Round 1), representing all 19 amino acid substitutions plus a stop codon in each of the 70 or 87 codons of the *gvpA* and *gvpB* genes, respectively. We constructed these libraries using a Golden Gate-based version of cassette mutagenesis,[26] in which mutagenic oligonucleotides that tile the gene of interest are synthesized and cloned into an acceptor vector (Figure S2A,B; see Methods Section for details). We chose this approach over error-prone polymerase chain reaction (PCR) because of its ability to generate defined libraries which have a controllable number of mutations per member and which lack unwanted mutants (*i.e.*, premature stop codons and multiple codons that code for the same mutant).

When induced in solid culture, these libraries produce three distinct types of colonies: (1) blue colonies, in which the dropout chromoprotein was not excised during assembly, returning the original acceptor vector; (2) low-opacity colonies that lack GV expression or express small amounts, either because they contain a mutant that reduces GV expression or because the mutant gene did not insert correctly during assembly; (3) high-opacity colonies with high GV expression. Colony opacity corresponds to GV expression because the low index of refraction of air inside GVs relative to surrounding aqueous media results in light scattering.[14,27] We used this readout to select only the mutants with high GV expression for further study. We then expressed these mutants (384 from each of the two libraries) in 96-well liquid cultures, and imaged them in the APR in 96-well agarose phantoms (Figures 1D and S1). Among the GvpA mutants, only a small number showed significantly higher nonlinear US signal than the WT (Figure 3C), while many GvpB mutants showed an increase (Figure 3D). This was likely because the GvpA construct fails to produce strongly opaque colonies when grown in solid culture, making it impossible to enrich for functional mutants prior to US screening; thus, the mutants screened *via* US from the GvpA library represent a random subset of the library, while those from the GvpB library are enriched for GV-producing sequences.

We chose up to 10 unique mutants with the highest US signal from each library and recloned them (see Methods Section) for validation and further characterization of their nonlinear acoustic signal (Figures 3E,F and S3A,B) and OD_{600} (Figure S3C,D). The top two mutants from each library—GvpA-T6A and -K22R, and GvpB-K22D and -S87I—generated nonlinear US signals 3.07-, 3.44-, 8.54-, and 7.41-fold higher than their parents, respectively, while growing to similar densities in liquid culture. The mutations found in the top 5 and top 10 variants from the GvpA and GvpB libraries, respectively, are shown in Figure 3G,H. These mutations cluster in the N-terminal linker and bridge domains, as well as

https://doi.org/10.1021/acssynbio.4c00283
ACS Synth. Biol. 2024, 13, 2215−2226

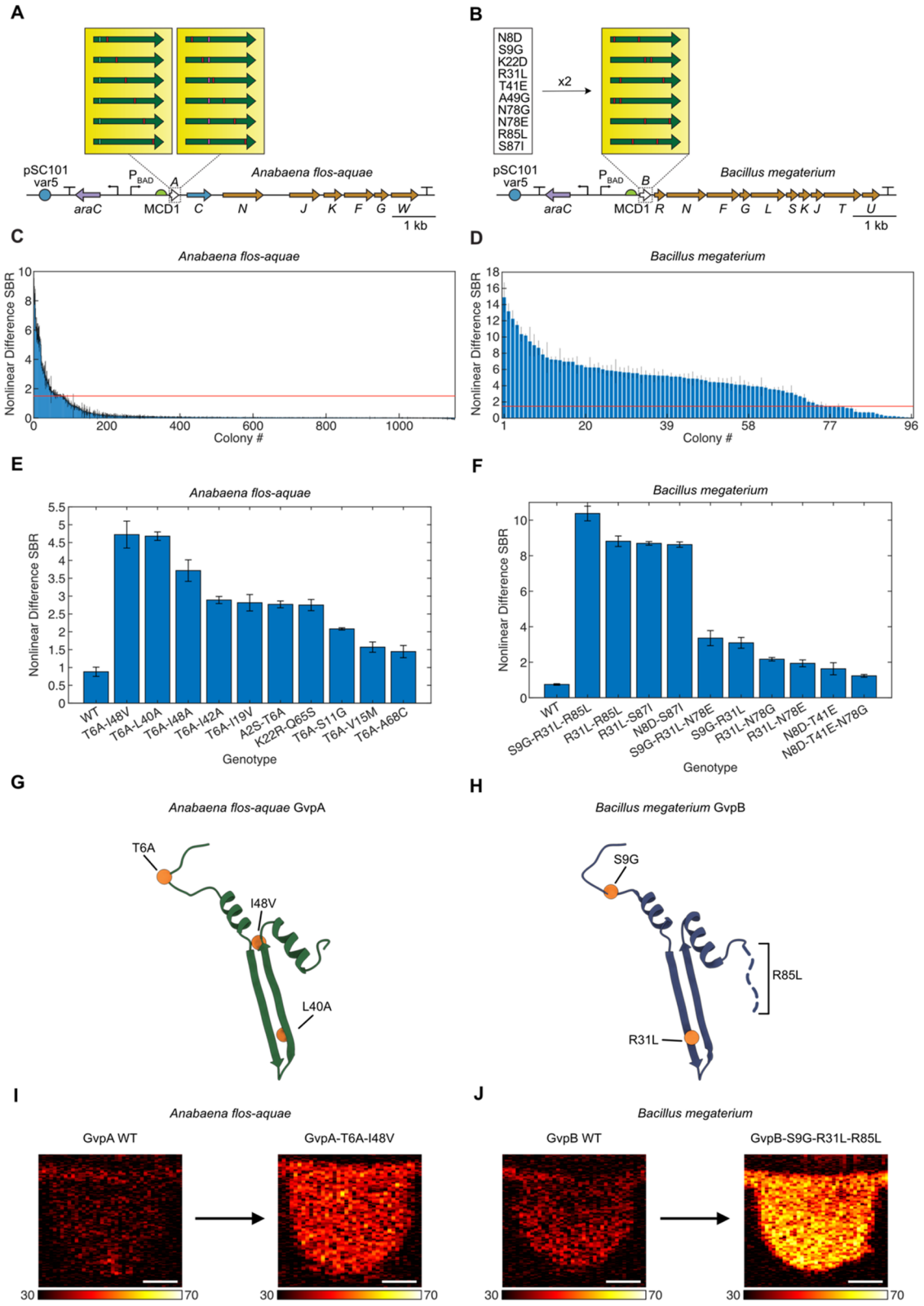

Figure 4. Second round of directed evolution of *A. flos-aquae* and *B. megaterium* structural proteins. (A, B) Diagrams of the mutagenized *A. flos-aquae* and *B. megaterium* gene clusters used in the second round of evolution. The best two mutants of *A. flos-aquae* gvpA were used as parents for another scanning site saturation library, and the best ten mutants of *B. megaterium* gvpB (listed in figure) were used to create a paired recombination library. (C, D) Nonlinear US difference signal-to-background ratio (SBR) from all screened mutants of both clusters. Red lines indicate the difference SBR of the WT for that cluster. Error bars represent standard error. $N = 3$ technical replicates of one biological sample. (E, F) Nonlinear US difference SBR for the WT and top ten mutants for each cluster. Error bars represent standard error. $N = 4$ biological samples (each an average of 3 technical replicates). (G, H) Locations of mutations from the top mutants from (E, F) in the GvpA/GvpB structure. (PDB 8GBS and 7R1C) (I, J) Representative nonlinear US images of the brightest mutants identified in this study, as well as their respective WT parents. Scale bars 1 mm. Color bar limits in decibels (dB).

https://doi.org/10.1021/acssynbio.4c00283
ACS Synth. Biol. 2024, 13, 2215−2226

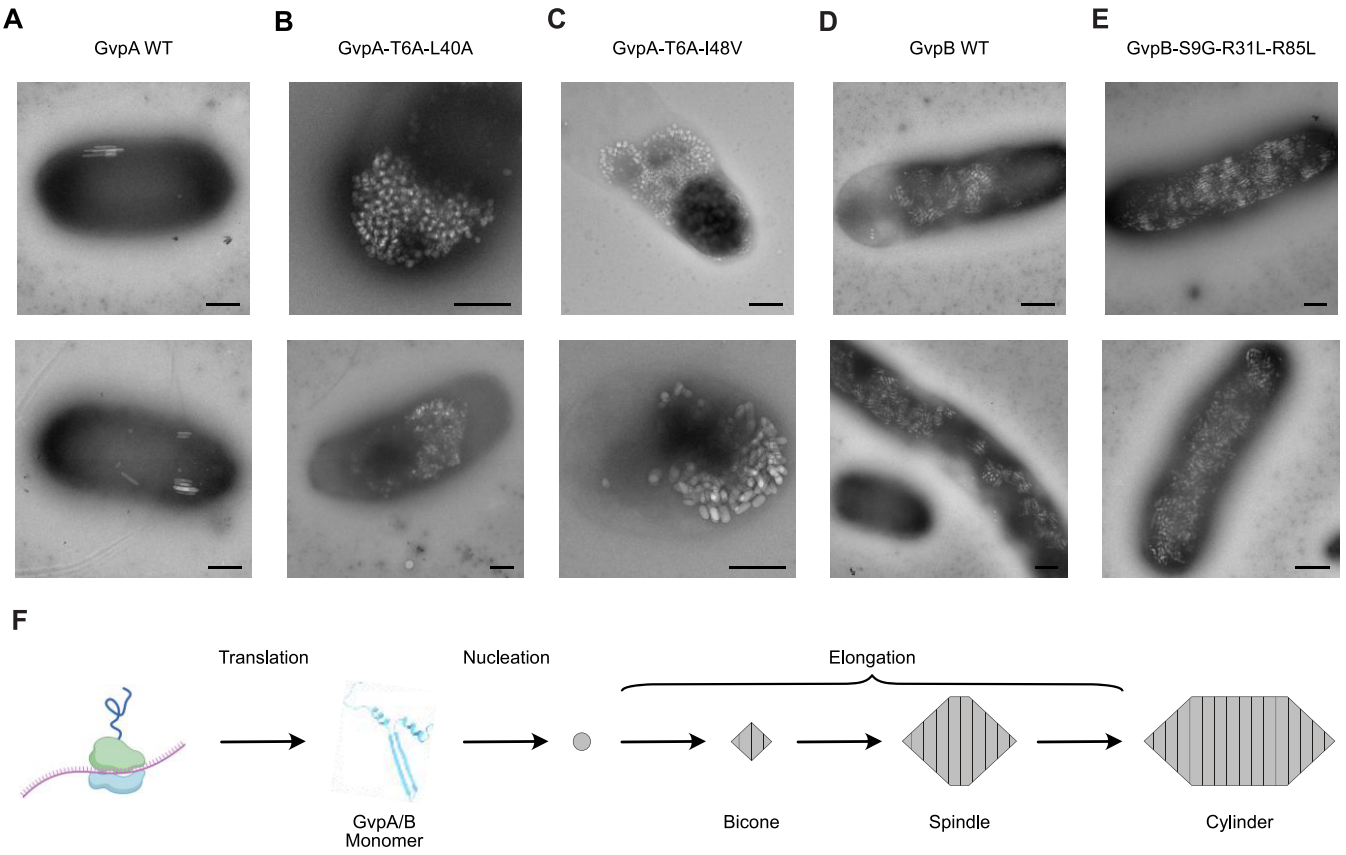

Figure 5. TEM of *E. coli* after expressing top-performing *A. flos-aquae* GvpA and *B. megaterium* GvpB mutants. (A–E) TEM images of WT and mutant GVs expressed in *E. coli*. (F) Diagram of the GV formation process. Scale bars 500 nm.

the hinge and wall domains, and the C-terminal tail.[16,17] Notably, no mutations occur in the C-terminal stabilization domain.

Round 2 Directed Evolution of *A. flos-aquae* GvpA and *B. megaterium* GvpB. We next performed a second round of directed evolution on these clusters by generating three distinct libraries: two scanning site saturation libraries of the top two mutants of *A. flos-aquae gvpA* (T6A and K22R) and a paired recombination library of the top 10 unique mutants of *B. megaterium gvpB* (Figure 4A,B) (though some members of this library contained three mutations due to a well-documented issue with amplifying oligonucleotide pools; see Methods Section for explanation). We cloned and screened these libraries using the same methods described for the first round of evolution (Figure 1D), and identified several mutants with greatly improved signal over their parents in both libraries (Figure 4C,D).

We characterized the top 10 unique mutants from each library in terms of their nonlinear acoustic signal (Figures 4E,F and S4A,B) and OD_{600} (Figure S4C,D), and identified GvpA-T6A-L40A, GvpA-T6A-I48V, and GvpB-S9G-R31L-R85L as the top-performing variants. These mutants generated nonlinear signals 5.32-, 5.37-, and 13.93-fold higher than their parents, respectively, while allowing the bacteria expressing them to grow to similar densities in liquid culture. The mutations found in the top 2 and top 1 variants from the second-round GvpA and GvpB libraries, respectively, are shown in Figure 4G,H. Similar to the mutations identified from the first-round libraries, these mutations cluster in the N-terminal linker domain, as well as the hinge and wall domains, and the C-terminal tail, but not the C-terminal stabilization domain.[16,17] Representative nonlinear US images of GvpA-T6A-L40A and GvpB-S9G-R31L-R85L, as well as the WT parents, are shown in Figure 4I,J. In addition to showing increased nonlinear contrast, the top variants have slightly higher collapse pressure than their WT parents when normalized for nonlinear contrast (Figure S5).

Expression Characteristics of Top Mutants. We performed whole-cell transmission electron microscopy (TEM) on *E. coli* expressing either WT or mutant ARGs to evaluate changes in expression levels. TEM revealed that these mutations increased the expression levels of both ARG types, either by increasing both the typical and maximum number of GVs per cell (in the case of GvpA-T6A-L40A and GvpA-T6A-I48V) or by making the number of GVs expressed per cell more consistent across all cells in the culture (in the case of GvpB-S9G-R31L-R85L) (Figures 5A–E, S6 and S7).

■ DISCUSSION

Our results establish the first method for high-throughput, semiautomated acoustic screening of biomolecules expressed in cells. When used to evolve two ARG clusters—those from *A. flos-aquae* and *B. megaterium*—this method yielded ARG constructs which show 5- to 14-fold improvements in their nonlinear acoustic scattering.

The mutations identified in this study appear to increase nonlinear US signal by increasing the maximum number of GVs produced per cell and/or making GV production more consistent across a cell population. These changes could be due to improved expression of GvpA/GvpB monomers or their

https://doi.org/10.1021/acssynbio.4c00283
ACS Synth. Biol. 2024, 13, 2215–2226

incorporation into growing GVs (Figure 5F). In addition, it is possible that some mutations contribute to increased nonlinear US scattering by individual GVs *via* changes to the mechanical properties of their shells.[11,21,22,28] While we did not directly assay for this effect, the fact that the acoustic collapse pressure increased for all mutants tested (Figure S5) suggests that some mechanical properties may be altered, but not necessarily in the direction of increased nonlinear contrast per GV. Thus, we attribute the majority of the observed changes in nonlinear US signal to increases in GV expression (Figure 5A−E). However, future screens could use an US signal that is only dependent on GV expression level (*e.g.*, BURST signal[29]) for normalization, to differentiate the contributions from increased expression level and from changes in shell mechanics.

These results represent a major advance in the way that acoustic biomolecules can be engineered. In the same way that high-throughput screening tools such as plate readers and flow cytometry enabled the engineering of fluorescent proteins and the many sensors derived from them by dramatically increasing the sizes of libraries that can be screened in these experiments, so too will the increased throughput, reliability, and standardization introduced by the Acoustic Plate Reader enable the engineering of next-generation ARGs and their derivatives.

While these evolved constructs represent substantial improvements over their parents, further improvements are required. First, both ARGs could benefit from further improvements in nonlinear contrast; this will likely be achieved through a combination of protein engineering (including not only the structural proteins engineered in this study, but also the assembly factors that assist in GV formation) and expression tuning (ORI, RBSs, and promoter) aimed at increasing both the amount of nonlinear contrast produced per GV and the number of GVs produced per cell. Relatedly, it would be desirable to engineer GVs with higher collapse pressures or ones whose collapse pressure is unchanged while having a significantly lower buckling threshold.

Additional engineering is needed to ensure the mutational stability of these constructs for *in vivo* applications, for example through chromosomal integration or inclusion of plasmid stability elements.[12] APR screening could facilitate any tuning required at the transcriptional (promoter) and translational (RBS) levels. Such tuning would potentially make the more compact *A. flos-aquae* and *B. megaterium*-derived ARGs competitive with the larger *Serratia*-derived ARGs, which currently provide the best *in vivo* imaging performance.[12] To further accelerate ARG development, we need a deeper understanding of how mutations to GvpA/GvpB affect both their structures[16,17] and the protein−protein interactions in which they participate during GV assembly,[30−33] as well as biochemical methods to characterize intermediate assembly steps that cannot be assayed by ultrasound, such as GV nucleation (Figure 5F).

By enabling the large-scale generation and high-throughput acoustic screening of ARG variants, the APR and its associated protocols allow the suite of modern protein engineering techniques to be applied to ARGs.

METHODS

Plasmid Construction *via* MoClo. The EcoFlex MoClo system[34] was used to create all vectors cloned in this study, including existing parts (Addgene Kit # 1000000080) and custom-made parts (Table S2). Custom-made parts were introduced into the existing EcoFlex system as follows: (1) ORIs were selected from the pSC101-varX series;[25] promoters were selected from the Marionette series;[35] RBSs were selected from the MCDX series;[36] terminators were selected from the ECK and LXSXPX series;[37] (2) parts were either synthesized as fragments (Twist Bioscience) and subsequently PCRed using Q5 (NEB), or synthesized as duplex oligos (IDT); (3) parts were cloned into the corresponding part entry vector (Table S2) *via* Golden Gate to ensure that they received the appropriate assembly overhangs. EcoFlex assemblies were conducted as described in Note S1 and electroporated into NEB Stable *E. coli* (except for the MetClo-based library acceptor vectors, which were transformed into DH10B-M.Osp807II[38]). Transformations were recovered for 2 h in 1 mL of SOC at 37 °C and 250 rpm, and plated on Petri dishes containing Lennox LB with 1% agar, 100 ug/mL kanamycin, and 1% glucose (for catabolite repression of the PBAD promoter). Colonies were picked into 1.5 mL liquid cultures of Lennox LB with 100 ug/mL kanamycin and 1% glucose in 96-well format and grown overnight to saturation. These cultures were then miniprepped using reagents and a protocol from Qiagen, a lysate clearing plate from Bio Basic (SD5006), and a DNA-binding plate from Epoch Life Sciences (2020−001). All constructs were verified by whole-plasmid sequencing (Primordium Laboratories).

Liquid Culture GV Expression in *E. coli*. GVs were expressed in *E. coli* liquid cultures in 96-well format according to the following general protocol, with modifications for specific experiments described below.

Miniprepped DNA was electroporated into NEB Stable *E. coli*, and transformations were recovered for 2 h at 37 °C in 1 mL of SOC. Transformations were then inoculated at a dilution of 1:100 into autoinduction Lennox LB containing 100 μg/mL kanamycin, 0.6% glycerol, and the appropriate concentrations of glucose and inducer for the experiment (see below). These expression cultures were set up in 500 μL volumes in deep-well 96-well plates (square wells were used for maximum culture aeration; USA Scientific 1896−2800) sealed with porous tape (Qiagen 19571) and incubated at 37 °C and 350 rpm for 20 h. Cultures were stored at 4C until being loaded into phantoms for Acoustic Plate Reader scans. For the concentrations of glucose and arabinose described below, in experiments where titrations were used, 100× stocks of these sugars were prepared in 1× phosphate-buffered saline (PBS) and diluted 1:100 into the cultures when setting up the experiments.

The following concentrations were used for the ORI titration experiments shown in Figure 2A−D: glucose: 0.25%; arabinose: 0, 0.0005, 0.001, 0.00155, 0.0025, 0.005, 0.01, 0.0155, 0.025, 0.05, 0.1, 0.25%.

The following concentrations were used for the parent expression optimization experiments shown in Figure 2E−J: glucose: 0, 0.1, 0.2, 0.3, 0.4, 0.5%; arabinose: 0, 0.0005, 0.001, 0.005, 0.01, 0.05, 0.1, 0.25%.

The following modifications were made for the library screening experiments shown in Figures 3A−D and 4A−D: (1) assembled libraries were transformed multiple times into NEB Stable *E. coli*, and it was ensured that the number of transformants produced was at least 100× the number of unique sequences expected in the library; (2) prior to expression in liquid culture, libraries were expressed in solid culture as colonies on Lennox LB with 100 ug/mL kanamycin, 0.6% glycerol, 0.25% glucose, and 0.05% arabinose at a density of ∼100 colonies/dish. Colonies were grown for 48 h at 37 °C,

https://doi.org/10.1021/acssynbio.4c00283
ACS Synth. Biol. 2024, 13, 2215−2226

and 380 opaque colonies were picked for each library, as well as 4 colonies for the library's parent, into the wells of 96-well PCR plates containing 100 μL of Lennox LB with 100 μg/mL kanamycin and 1% glucose, and grown to saturation overnight at 30 °C. These saturated liquid cultures, rather than transformations, were used to set up expression cultures as described above; (3) 0.25% glucose, and 0.05% arabinose were used to induce expression in these experiments.

The following concentrations were used for the mutant expression experiments shown in Figures 3E−F and 4E−F and S3−S5: glucose: 0.25%; arabinose: 0.05%.

The following concentrations were used for the TEM experiments shown in Figure 5A−E and S6−S7: glucose: 0.25%; arabinose: 0.05%.

Scanning Site Saturation and Recombination Library Generation. Scanning site saturation libraries were generated *via* a Golden Gate-based version of the cassette mutagenesis strategy previously described.[39] Briefly, the *A. flos-aquae* GvpA and *B. megaterium* GvpB coding sequences were divided into sections that tiled the gene, and oligos were designed to have a variable middle region with flanking constant regions against which PCR primers were designed (these primers also contain the evSeq[40] inner adapters for optional deep sequencing of the library) (Figure S2A). Depending on the library being created (*i.e.*, scanning site saturation or recombination), the variable region was designed to either sequentially saturate each residue or recombine pairs of the mutations listed in Figure 4B (mutations identified during screening of the first round of scanning site saturation of GvpB). The MATLAB scripts used to generate the oligo sequences for both the scanning site saturation and recombination libraries are available in Codes S1 and S2, and the oligo sequences themselves are listed in Table S1. Oligos were synthesized as a pool by Twist Biosciences or Integrated DNA Technologies, and were amplified by PCR (both to make them double-stranded and to generate enough DNA for Golden Gate assembly) using KAPA HiFi HotStart ReadyMix according to the manufacturer's instructions, but with 10 cycles, 100 ng of oligo pool template, and 1 uM of each primer. PCR products were run on a 2% agarose gel and purified using Qiagen reagents according to the manufacturer's instructions, but with a 5 μL final elution volume of water. Fragments were then assembled with the corresponding library acceptor vector (Table S2) in a Golden Gate reaction using reagents from New England Biolabs according to the manufacturer's instructions. Assemblies were then expressed (first in solid culture and then in liquid culture) according to the protocol above.

It is important to note that oligo pools whose members have very high sequence similarity (as was the case in the pools used in this study, in which members differed by only a few bp) have a high likelihood of mutation swapping during PCR which increases with the number of cycles used. The manufacturer proposes that this is due to template swapping from one cycle to the next between incompletely copied strands. We notice this often in our libraries (*i.e.*, libraries synthesized to have two mutations per member would contain a small number of sequences with zero or three mutations per member after PCR), and we minimized the number of PCR cycles used to amplify these libraries. However, some of the best round 2 GvpB mutants contained three mutations for this reason.

Acoustic Plate Reader Scans. The general protocol for preparing and scanning liquid cultures samples of GV-expressing *E. coli* in 96-well format is described in Figure S1 and the corresponding figure caption. Detailed instructions on how to build and use this system, as well as troubleshooting and bug-reporting information, are provided at https://github.com/shapiro-lab/acoustic-plate-reader.

The specific US pulse sequence parameters used for collecting the data shown in each figure are presented in Table S3.

For pre/postcollapse and voltage ramp scans, the nonlinear difference SBR was calculated as [(precollapse sample mean) − (postcollapse sample mean)]/(postcollapse background mean), where means are calculated from the nonlinear signal in a region of interest containing either the sample or an empty region of the phantom. For voltage ramp scans, this quantity was calculated for each precollapse image; for simple pre/postcollapse scans, this quantity was calculated only once for the single precollapse image. Importantly, in all cases the two images being compared in each calculation were acquired at the same voltage (*i.e.*, the pre- and postcollapse images were collected under the same imaging conditions).

For collapse ramp scans, the nonlinear SBR was calculated as (sample mean)/(background mean), where means are calculated from the nonlinear signal in a region of interest containing either the sample or an empty region of the phantom. This quantity was calculated for each image at each voltage.

Validation of Best Mutants. Selected mutants from each library were miniprepped and sequenced as described above. Unique mutants were then recloned using MoClo (see above) before undergoing validation testing to avoid the possibility that these plasmids accrued expression-reducing mutations during the GV expression steps performed during library screening. To prepare fragments for these MoClo assemblies, *gvpA*/*gvpB* mutant CDSs were PCRed using the primers described in Table S4 (which were selected based on the sequence of the mutant being amplified) and prepared for Golden Gate assembly as described above.

OD_{600} Measurements. OD_{600} culture measurements were performed on a Tecan Spark plate reader using the "Absorbance" protocol with the following settings: 600 nm measurement wavelength, 10 flashes, 50 ms settle time. Measurements were collected for 200 μL of culture and normalized to a 1 cm path length using the built-in "Pathlength Correction" feature.

Negative Stain TEM Imaging. Three microliters of *E. coli* culture expressing GVs were applied to a freshly glow-discharged (Pelco EasiGlow, 15 mA, 1 min) Formvar/carbon-coated, 200-mesh copper grid (Ted Pella), and then incubated for 1 min. Excess solution was blotted with filter paper, and the grids were washed 3 times with buffer (20 mM HEPES buffer; pH 7.5, 100 mM NaCl). Subsequently, the sample was stained with a 2% uranyl acetate solution for 1 min, blotted, and air-dried. Images were acquired using a Tecnai T12 electron microscope (FEI, now Thermo Fisher Scientific) operating at 120 kV and equipped with a Gatan Ultrascan 2k × 2k CCD.

■ ASSOCIATED CONTENT

Data Availability Statement

Selected plasmids are available through Addgene (202023, 202024, 202025). Detailed instructions on how to build and use the Acoustic Plate Reader, as well as troubleshooting and bug-reporting information, are provided at https://github.

https://doi.org/10.1021/acssynbio.4c00283
ACS Synth. Biol. 2024, 13, 2215−2226

com/shapiro-lab/acoustic-plate-reader. All other data and code are available from the corresponding author upon reasonable request.

Supporting Information

The Supporting Information is available free of charge at https://pubs.acs.org/doi/10.1021/acssynbio.4c00283.

Supplementary Video 1: Example acoustic plate reader scan. (Right) The Acoustic Plate Reader is scanning six 96-well phantoms; (left) the computer screen displays the real-time images of linear (left) and nonlinear (middle) contrast, as well as the Verasonics control interface (right) (MP4)

Table S1: Oligos used for mutagenesis. Sequences of the oligos that composed the four oligo pools used to create the GvpA/GvpB libraries. "Library Round" indicates the round of screening (first or second) in which the oligo was used, and "Sub-Library" indicates the pool in which it was synthesized; Table S2: Custom-made MoClo parts. Inventory of the MoClo parts added to the base EcoFlex system and used for cloning the constructs in this study; Table S3: Ultrasound pulse sequences. List of the parameters entered into the APR GUI to perform each scan in this study; Table S4: PCR primers. Sequences of the primers used to either amplify the oligo pools that were used to create the libraries, or to reclone the best *gvpA/gvpB* mutants into Level 0 MoClo part vectors for assembly into expression constructs and subsequent validation (XLSX)

Detailed diagram of the Acoustic Plate Reader workflow; details of *gvpA/gvpB* mutant library construction; characterization of the top mutants from Rounds 1 and 2 of evolution; acoustic collapse pressure curves for the best mutants identified in this study; TEM images of *E. coli* cells expressing WT or mutant *A. flos-aquae* GVs; TEM images of *E. coli* cells expressing WT or mutant *B. megaterium* GVs; Golden Gate reaction parameters (PDF)

Code S1: MATLAB script and associated files for generating the scanning site saturation libraries (ZIP)

Code S2: MATLAB script and associated files for generating the recombination library (ZIP)

AUTHOR INFORMATION

Corresponding Author

Mikhail G. Shapiro − *Andrew and Peggy Cherng Department of Medical Engineering, Division of Chemistry and Chemical Engineering, and Howard Hughes Medical Institute, California Institute of Technology, Pasadena, California 91125, United States;* orcid.org/0000-0002-0291-4215; Phone: 626-395-8588; Email: mikhail@caltech.edu

Authors

Robert C. Hurt − *Division of Biology and Biological Engineering, California Institute of Technology, Pasadena, California 91125, United States;* orcid.org/0000-0002-4347-6901

Zhiyang Jin − *Andrew and Peggy Cherng Department of Medical Engineering, California Institute of Technology, Pasadena, California 91125, United States;* orcid.org/0000-0002-4411-6991

Mohamed Soufi − *Division of Chemistry and Chemical Engineering, California Institute of Technology, Pasadena, California 91125, United States*

Katie K. Wong − *Division of Chemistry and Chemical Engineering, California Institute of Technology, Pasadena, California 91125, United States*

Daniel P. Sawyer − *Division of Biology and Biological Engineering, California Institute of Technology, Pasadena, California 91125, United States*

Hao K. Shen − *Division of Chemistry and Chemical Engineering, California Institute of Technology, Pasadena, California 91125, United States;* orcid.org/0000-0003-2687-0736

Przemysław Dutka − *Division of Biology and Biological Engineering and Division of Chemistry and Chemical Engineering, California Institute of Technology, Pasadena, California 91125, United States*

Ramya Deshpande − *Division of Chemistry and Chemical Engineering, California Institute of Technology, Pasadena, California 91125, United States*

Ruby Zhang − *Division of Chemistry and Chemical Engineering, California Institute of Technology, Pasadena, California 91125, United States*

David R. Mittelstein − *Andrew and Peggy Cherng Department of Medical Engineering, California Institute of Technology, Pasadena, California 91125, United States*

Complete contact information is available at: https://pubs.acs.org/10.1021/acssynbio.4c00283

Author Contributions

⊥R.C.H. and Z.J. contributed equally to this work. R.C.H., Z.J., and M.G.S. conceived and designed the study. Z.J. and D.R.M. designed and built the Acoustic Plate Reader hardware. Z.J., D.P.S., and D.R.M. wrote the MATLAB scripts for data acquisition with the Acoustic Plate Reader. R.C.H., Z.J., and D.P.S. wrote the MATLAB scripts for data analysis from the Acoustic Plate Reader. M.S. designed the MATLAB graphical user interfaces for Acoustic Plate Reader data acquisition and analysis. R.C.H., M.S., K.W., H.K.S., R.D., and R.Z. performed directed evolution experiments. P.D. performed TEM imaging. R.C.H. analyzed all data. R.C.H. wrote the paper, with input from all authors. M.G.S. supervised the research.

Notes

The authors declare no competing financial interest.

ACKNOWLEDGMENTS

The authors would like to thank Rohit Nayak for providing calibration data for the US transducer used for imaging. Transmission electron microscopy was done in the Beckman Institute Resource Center for Transmission Electron Microscopy at Caltech. This research was supported by the National Institutes of Health (R01-EB018975 to M.G.S.), the Chan-Zuckerberg Initiative and Pew Charitable Trust. R.C.H. was supported by the Caltech Center for Environmental Microbial Interactions. Related research in the Shapiro Laboratory is supported by the David and Lucile Packard Foundation. M.G.S. is an investigator of the Howard Hughes Medical Institute.

ABBREVIATIONS

US: ultrasound
GV: gas vesicle

ARG: acoustic reporter gene
APR: acoustic plate reader
SBR: signal-to-background ratio

REFERENCES

(1) Bourdeau, R. W.; Lee-Gosselin, A.; Lakshmanan, A.; Farhadi, A.; Kumar, S. R.; Nety, S. P.; Shapiro, M. G. Acoustic reporter genes for noninvasive imaging of microorganisms in mammalian hosts. *Nature* **2018**, *553*, 86−90.

(2) Farhadi, A.; Ho, G. H.; Sawyer, D. P.; Bourdeau, R. W.; Shapiro, M. G. Ultrasound imaging of gene expression in mammalian cells. *Science* **2019**, *365*, 1469−1475.

(3) Pfeifer, F. Distribution, formation and regulation of gas vesicles. *Nat. Rev. Microbiol.* **2012**, *10*, 705−715.

(4) Walsby, A. E. Gas vesicles. *Microbiol. Rev.* **1994**, *58*, 94−144.

(5) Shapiro, M. G.; Goodwill, P. W.; Neogy, A.; Yin, M.; Foster, F. S.; Schaffer, D. V.; Conolly, S. M. Biogenic gas nanostructures as ultrasonic molecular reporters. *Nat. Nanotechnol.* **2014**, *9*, 311−316.

(6) Ling, B.; Lee, J.; Maresca, D.; Lee-Gosselin, A.; Malounda, D.; Swift, M. B.; Shapiro, M. G. Biomolecular Ultrasound Imaging of Phagolysosomal Function. *ACS Nano* **2020**, *14*, 12210−12221.

(7) Jin, Z.; Lakshmanan, A.; Zhang, R.; Tran, T. A.; Rabut, C.; Dutka, P.; Duan, M.; Hurt, R. C.; Malounda, D.; Yao, Y.; Shapiro, M. G. Ultrasonic reporters of calcium for deep tissue imaging of cellular signals. preprint *Bioengineering* 2023.

(8) Yang, G.; Withers, S. G. Ultrahigh-Throughput FACS-Based Screening for Directed Enzyme Evolution. *ChemBioChem* **2009**, *10*, 2704−2715.

(9) Kazlauskas, R. J.; Bornscheuer, U. T. Finding better protein engineering strategies. *Nat. Chem. Biol.* **2009**, *5*, 526−529.

(10) Packer, M. S.; Liu, D. R. Methods for the directed evolution of proteins. *Nat. Rev. Genet.* **2015**, *16*, 379−394.

(11) Maresca, D.; Lakshmanan, A.; Lee-Gosselin, A.; Melis, J. M.; Ni, Y.-L.; Bourdeau, R. W.; Kochmann, D. M.; Shapiro, M. G. Nonlinear ultrasound imaging of nanoscale acoustic biomolecules. *Appl. Phys. Lett.* **2017**, *110*, No. 073704.

(12) Hurt, R. C.; Buss, M. T.; Duan, M.; Wong, K.; You, M. Y.; Sawyer, D. P.; Swift, M. B.; Dutka, P.; Barturen-Larrea, P.; Mittelstein, D. R.; Jin, Z.; Abedi, M. H.; Farhadi, A.; Deshpande, R.; Shapiro, M. G. Genomically mined acoustic reporter genes for real-time in vivo monitoring of tumors and tumor-homing bacteria. *Nat. Biotechnol.* **2023**, *41*, 919−931.

(13) Lakshmanan, A.; Jin, Z.; Nety, S. P.; Sawyer, D. P.; Lee-Gosselin, A.; Malounda, D.; Swift, M. B.; Maresca, D.; Shapiro, M. G. Acoustic biosensors for ultrasound imaging of enzyme activity. *Nat. Chem. Biol.* **2020**, *16*, 988−996.

(14) Lu, G. J.; Chou, L.; Malounda, D.; Patel, A. K.; Welsbie, D. S.; Chao, D. L.; Ramalingam, T.; Shapiro, M. G. Genetically Encodable Contrast Agents for Optical Coherence Tomography. *ACS Nano* **2020**, *14*, 7823−7831.

(15) Li, N.; Cannon, M. C. Gas vesicle genes identified in *Bacillus megaterium* and functional expression in *Escherichia coli*. *J. Bacteriol.* **1998**, *180*, 2450−2458.

(16) Huber, S. T.; Terwiel, D.; Evers, W. H.; Maresca, D.; Jakobi, A. J. Cryo-EM structure of gas vesicles for buoyancy-controlled motility. *Cell* **2023**, *186*, 975−986.e13.

(17) Dutka, P.; Metskas, L. A.; Hurt, R. C.; Salahshoor, H.; Wang, T.-Y.; Malounda, D.; Lu, G. J.; Chou, T.-F.; Shapiro, M. G.; Jensen, G. J. Structure of *Anabaena flos-aquae* gas vesicles revealed by cryo-ET. *Structure* **2023**, *31*, 518−528.e6.

(18) Lakshmanan, A.; Farhadi, A.; Nety, S. P.; Lee-Gosselin, A.; Bourdeau, R. W.; Maresca, D.; Shapiro, M. G. Molecular Engineering of Acoustic Protein Nanostructures. *ACS Nano* **2016**, *10*, 7314−7322.

(19) Rabut, C.; Wu, D.; Ling, B.; Jin, Z.; Malounda, D.; Shapiro, M. G. Ultrafast amplitude modulation for molecular and hemodynamic ultrasound imaging. *Appl. Phys. Lett.* **2021**, *118*, No. 244102.

(20) Zhang, S.; Huang, A.; Bar-Zion, A.; Wang, J.; Mena, O. V.; Shapiro, M. G.; Friend, J. The Vibration Behavior of Sub-Micrometer Gas Vesicles in Response to Acoustic Excitation Determined via Laser Doppler Vibrometry. *Adv. Funct. Mater.* **2020**, *30*, No. 2000239.

(21) Maresca, D.; Sawyer, D. P.; Renaud, G.; Lee-Gosselin, A.; Shapiro, M. G. Nonlinear X-Wave Ultrasound Imaging of Acoustic Biomolecules. *Phys. Rev. X* **2018**, *8*, No. 041002.

(22) Cherin, E.; Melis, J. M.; Bourdeau, R. W.; Yin, M.; Kochmann, D. M.; Foster, F. S.; Shapiro, M. G. Acoustic Behavior of Halobacterium salinarum Gas Vesicles in the High-Frequency Range: Experiments and Modeling. *Ultrasound Med. Biol.* **2017**, *43*, 1016−1030.

(23) Maresca, D.; Lakshmanan, A.; Abedi, M.; Bar-Zion, A.; Farhadi, A.; Lu, G. J.; Szablowski, J. O.; Wu, D.; Yoo, S.; Shapiro, M. G. Biomolecular Ultrasound and Sonogenetics. *Annu. Rev. Chem. Biomol. Eng.* **2018**, *9*, 229−252.

(24) Lakshmanan, A.; Lu, G. J.; Farhadi, A.; Nety, S. P.; Kunth, M.; Lee-Gosselin, A.; Maresca, D.; Bourdeau, R. W.; Yin, M.; Yan, J.; Witte, C.; Malounda, D.; Foster, F. S.; Schröder, L.; Shapiro, M. G. Preparation of biogenic gas vesicle nanostructures for use as contrast agents for ultrasound and MRI. *Nat. Protoc.* **2017**, *12*, 2050−2080.

(25) Segall-Shapiro, T. H.; Sontag, E. D.; Voigt, C. A. Engineered promoters enable constant gene expression at any copy number in bacteria. *Nat. Biotechnol.* **2018**, *36*, 352−358.

(26) Wells, J. A.; Vasser, M.; Powers, D. B. Cassette mutagenesis: an efficient method for generation of multiple mutations at defined sites. *Gene* **1985**, *34*, 315−323.

(27) Farhadi, A.; Bedrossian, M.; Lee, J.; Ho, G. H.; Shapiro, M. G.; Nadeau, J. L. Genetically Encoded Phase Contrast Agents for Digital Holographic Microscopy. *Nano Lett.* **2020**, *20*, 8127−8134.

(28) Salahshoor, H.; Yao, Y.; Dutka, P.; Nyström, N. N.; Jin, Z.; Min, E.; Malounda, D.; Jensen, G. J.; Ortiz, M.; Shapiro, M. G. Geometric effects in gas vesicle buckling under ultrasound. *Biophys. J.* **2022**, *121*, 4221−4228.

(29) Sawyer, D. P.; Bar-Zion, A.; Farhadi, A.; Shivaei, S.; Ling, B.; Lee-Gosselin, A.; Shapiro, M. G. Ultrasensitive ultrasound imaging of gene expression with signal unmixing. *Nat. Methods* **2021**, *18*, 945−952.

(30) Iburg, M.; Anderson, A. P.; Wong, V. T.; Anton, E. D.; He, A.; Lu, G. J. Elucidating the Assembly of Gas Vesicles by Systematic Protein-Protein Interaction Analysis *Biology* 2023.

(31) Jost, A.; Pfeifer, F. Interaction of the gas vesicle proteins GvpA, GvpC, GvpN, and GvpO of Halobacterium salinarum. *Front. Microbiol.* **2022**, *13*, No. 971917.

(32) Völkner, K.; Jost, A.; Pfeifer, F. Accessory Gvp Proteins Form a Complex During Gas Vesicle Formation of Haloarchaea. *Front. Microbiol.* **2020**, *11*, No. 610179.

(33) Winter, K.; Born, J.; Pfeifer, F. Interaction of Haloarchaeal Gas Vesicle Proteins Determined by Split-GFP. *Front. Microbiol.* **2018**, *9*, No. 1897.

(34) Moore, S. J.; Lai, H.-E.; Kelwick, R. J. R.; Chee, S. M.; Bell, D. J.; Polizzi, K. M.; Freemont, P. S. EcoFlex: A Multifunctional MoClo Kit for *E. coli* Synthetic Biology. *ACS Synth. Biol.* **2016**, *5*, 1059−1069.

(35) Meyer, A. J.; Segall-Shapiro, T. H.; Glassey, E.; Zhang, J.; Voigt, C. A. *Escherichia coli* "Marionette" strains with 12 highly optimized small-molecule sensors. *Nat. Chem. Biol.* **2019**, *15*, 196−204.

(36) Mutalik, V. K.; Guimaraes, J. C.; Cambray, G.; Lam, C.; Christoffersen, M. J.; Mai, Q.-A.; Tran, A. B.; Paull, M.; Keasling, J. D.; Arkin, A. P.; Endy, D. Precise and reliable gene expression via standard transcription and translation initiation elements. *Nat. Methods* **2013**, *10*, 354−360.

(37) Chen, Y.-J.; Liu, P.; Nielsen, A. A. K.; Brophy, J. A. N.; Clancy, K.; Peterson, T.; Voigt, C. A. Characterization of 582 natural and synthetic terminators and quantification of their design constraints. *Nat. Methods* **2013**, *10*, 659−664.

(38) Lin, D.; O'Callaghan, C. A. MetClo: methylase-assisted hierarchical DNA assembly using a single type IIS restriction enzyme. *Nucleic Acids Res.* **2018**, No. e113.

(39) Ravikumar, A.; Arzumanyan, G. A.; Obadi, M. K. A.; Javanpour, A. A.; Liu, C. C. Scalable, Continuous Evolution of Genes at Mutation

https://doi.org/10.1021/acssynbio.4c00283
ACS Synth. Biol. 2024, 13, 2215−2226

Rates above Genomic Error Thresholds. *Cell* **2018**, *175*, 1946−1957.e13.
(40) Wittmann, B. J.; Johnston, K. E.; Almhjell, P. J.; Arnold, F. H. evSeq: Cost-Effective Amplicon Sequencing of Every Variant in a Protein Library. *ACS Synth. Biol.* **2022**, *11*, 1313−1324.

https://doi.org/10.1021/acssynbio.4c00283
ACS Synth. Biol. 2024, 13, 2215−2226